



Acoustic monitoring of O₂ production of a seagrass meadow



Paulo Felisberto^{a,*}, Sérgio M. Jesus^a, Friedrich Zabel^b, Rui Santos^c, João Silva^c, Sylvie Gobert^d, Sven Beer^e, Mats Björk^f, Silvia Mazzuca^g, Gabriele Procaccini^h, John W. Runcieⁱ, Willy Champenois^j, Alberto V. Borges^j

^a LARSyS, University of Algarve, Faro, Portugal

^b MarSensing Lda, Faro, Portugal

^c Marine Plant Ecology Research Group, Center of Marine Sciences (CCMar), University of Algarve, Faro, Portugal

^d Laboratory of Oceanology - MARE Centre, University of Liège, Belgium

^e Department of Plant Sciences, Tel Aviv University, Tel Aviv, Israel

^f Department of Ecology, Environment and Plant Sciences, Stockholm University, Stockholm, Sweden

^g Department of Chemistry and Technology, University of Calabria, Rende, Italy

^h Stazione Zoologica Anton Dohrn, Naples, Italy

ⁱ School of Biological Sciences, University of Sydney, Sydney, Australia

^j Chemical Oceanography Unit, University of Liège, Belgium

ARTICLE INFO

Article history:

Received 15 August 2014

Received in revised form 17 December 2014

Accepted 28 December 2014

Available online xxx

Keywords:

Acoustic data

Oxygen

Primary production

Seagrass

ABSTRACT

Acoustic data were acquired in October 2011 over a *Posidonia oceanica* meadow in the Bay of la Revellata, Calvi, Corsica. The purpose was to develop an acoustic system for monitoring the oxygen (O₂) production of an entire seagrass meadow. In a shallow water area (<38 m), densely covered by *P. oceanica*, a sound source transmitted signals in 3 different bands (400–800 Hz, 1.5–3.5 kHz and 6.5–8.5 kHz) toward three self-recording hydrophones at a distance of 100 m, over the period of one week. The data show a high correlation between the diel cycle of the acoustic signals' energy received by the hydrophones and the temporal changes in water column O₂ concentration as measured by optodes. The results thus show that a simple acoustic acquisition system can be used to monitor the O₂-based productivity of a seagrass meadow at the ecosystem level with high temporal resolution. The finding of a significant production of O₂ as bubbles in seagrass ecosystems suggests that net primary production is underestimated by methods that rely on the mass balance of dissolved O₂ measurements.

© 2015 Elsevier B.V. All rights reserved.

1. Introduction

Long term and continuous measurements of relevant parameters of ecosystem metabolism in coastal areas with high spatial coverage and high time resolution are of primary importance for ecosystem health assessment and, in turn, for sustainable management. Seagrass-dominated ecosystems provide valued ecosystem goods and services (Costanza et al., 1997), that are among the most productive biomes on earth (Duarte et al., 2010), and sequester large quantities of carbon (Mcleod et al., 2011). Seagrasses are, however, declining worldwide, and the need for integrative management practices is emerging (Waycott et al., 2009).

Several methods have been used to estimate the amount of oxygen (O₂) produced by a seagrass ecosystem which is an important parameter for assessing its metabolism and productivity (Silva et al., 2009); (Staeher et al., 2011); (Champenois and Borges, 2012). Whole-community metabolism based on O₂ measurements can be determined using incubation chambers for individual plant assemblages. Open water method measurements of diel changes in O₂ concentrations, or

oxygen isotopes (Staeher et al., 2011), are used on the ecosystem level. Open water methods include O₂ input–output mass balance (Gazeau et al., 2005), diel cycle mass balance, i.e. the Odum (1956) method (Champenois and Borges, 2012), and eddy covariance (Chipman et al., 2012). Incubation chambers provide a direct and precise local measurement of O₂ exchange between the organisms and the surrounding water either via electrodes or chemically by Winkler titration, but they have the caveat of being discrete temporal and spatial measurements (Silva et al., 2009); (Staeher et al., 2011). For such measurements, O₂ optodes provide for optical detection, and are much more stable with time than the older Clark-type O₂ electrodes (Tengberg et al., 2006). The input–output mass balance approach also requires a large number of O₂ profiles from ships or moorings and data on water transport, while eddy covariance methods are not at present possible on long deployments due to limitations of sensors (Chipman et al., 2012).

In general, acoustic signals propagating through seawater are sensitive to seabed properties (Medwin and Clay, 1998). The influence of seagrass beds in the statistical distribution of scattered amplitude of high frequency signals (>20 kHz) were investigated by Lyons and Abraham (1999) and McCarthy and Sabol (2000). The usage of high frequency acoustics for mapping submerged aquatic vegetation, and seagrasses in particular, was also demonstrated. Echosounders, side-

* Corresponding author. Tel.: +351 289800900; fax: +351 289888405.
E-mail address: pfelis@ualg.pt (P. Felisberto).

scan sonars and acoustic Doppler current profilers have been used to characterize estuarine bottom habitat type and to estimate plant abundance, biomass and canopy height (Warren and Peterson, 2007).

Seagrass meadows are highly productive ecosystems; thus the concentration of dissolved O₂ and bubbles produced by photosynthesis changes significantly during the diel cycle. It is well known (Medwin and Clay, 1998) that the concentration and size of the bubbles affect sound propagation to a much greater extent than dissolved O₂. Hermand et al. (2000) and Hermand (2004) showed that signatures in low frequency acoustic signals (<16 kHz) transmitted (horizontally) through *Posidonia oceanica* meadows were highly correlated with the O₂ produced by the plants during photosynthesis. During the day (photosynthetic activity) the channel impulse responses showed higher attenuation of received echoes than during the night, which corresponded to a decrease of received energy. Wilson et al. (2012) studied the propagation of high frequency signals (100 kHz), through stands of the seagrasses *Syringodium filiforme*, *Halodule wrightii* and *Thalassia testudinum*. It was a small scale experiment conducted in an outdoor mesocosm. The source receiver range and the water depth was only 0.54 m. It was observed for all tested species that the energy of the received signal varied about 4 dB over a 24-h period. While for *S. filiforme* the attenuation of the signal was positively correlated with available photosynthetically active radiation (PAR), for *H. wrightii* it was negatively correlated, and no correlation was identified for *T. testudinum*.

The factors that influence the acoustic response of a seagrass are not well established, but it is considered that free gas bubbles emanating from the plants and the pressurization of the aerenchyma by photosynthetic O₂ production are the most relevant ones. At frequencies well below the bubbles resonance frequency, both factors influence the acoustic compressibility and, thus, the effective sound speed of the medium (Hermand et al., 2000); (Wilson and Dunton, 2009); (Wilson et al., 2010, 2012). Attempts to quantify the effective sound speed of the seagrass environment through an effective medium model, such as Wood's equation (Wilson et al., 2010), have been shown to be inadequate. Despite these modeling difficulties, the often found positive correlation between photosynthesis and the attenuation of low frequency signals is ascribed to a low speed sound channel that develops at the seagrass bed and is modulated by bubble concentration (Hermand et al., 2000); (Hermand, 2004).

The present study, using a similar approach to that of Hermand et al. (2000); Hermand (2004) and Wilson et al. (2012), discusses the problem of selecting a convenient frequency band of the probe signal in order to attain a higher dependence of the signal on photosynthetic O₂ production when compared with other environmental parameters. The signals in this frequency band will minimize the relative influence of other environmental parameters that affect sound propagation like temperature changes and tidal effects, among others, allowing for simpler and more robust acoustic methods to estimate the O₂ concentration. The influence of the frequency band of the probe signal will be illustrated with the results obtained from signals in three different bands: 400–800 Hz, 1500–3500 Hz and 6500–8500 Hz. The correlation between the acoustic data and dissolved O₂ measurements from an array of 3 optodes is also validated, showing the potential usage of acoustics as a proxy for the dynamics of seagrass O₂ metabolism at ecosystem level. In doing so, the present work thus focusses on the acoustic data of an interdisciplinary experiment devoted to the study of seagrass metabolism with different methods, at different spatial and temporal scales (Mazzuca et al., 2013).

2. Materials and methods

2.1. The study area

The experiment was conducted from October 10 to 19, 2011, in a *P. oceanica* (L.) Delile meadow in front of the Station de Recherches Sous-marine et Océanographiques (STARESO), Calvi, Corsica. This is an

oligotrophic area classified as a pristine site, where a healthy and dense *P. oceanica* meadow extends from approximately 5 m to 38 m water depth. In the Bay of la Revellata the depth of the mixed layer varies between 25 m in summer and more than 100 m in winter, whereas the seawater temperature ranges from 13 °C in late winter to 26 °C in late summer (Bay, 1984). The salinity is virtually constant at 38 ppt (Hecq et al., 1986). Gobert et al. (2003) characterized the spatial variation of several biometric parameters of the meadow, showing that the shoot density decreases linearly with depth (from about 500 shoots m⁻² at 5 m to 100 shoots m⁻² at 30 m), while the number of leaves per shoot does not change significantly with depth (about 6 leaves per shoot). In October 2011, the height of the canopy was 67 ± 15 cm, 59 ± 14 cm and 79 ± 7 cm at 5, 10 and 20 m depth, respectively (Gobert et al., 2012). The height of the canopy is the mean of the maximum leaf length of ten shoots measured in situ with a tape-line.

Champenois and Borges (2012) measured the O₂ production in this meadow during a period of three years, from August 2006 to October 2009, with an array of three optodes installed at a water depth of 10 m. The maximum overall value of 25 g O₂ m⁻² day⁻¹ was observed in midsummer, whereas the highest value in February reached 5.4 g O₂ m⁻² day⁻¹.

2.2. The acoustic experiment setup

The acoustic monitoring system comprised a sound source installed close to the STARESO pier at a water depth of 8.5 m, and 3 self-recording hydrophones moored at a water depth of 21.5 m. The transmissions were performed along the bathymetric slope to cover the area of interest of the interdisciplinary experiment (Mazzuca et al., 2013). The working area and the position of the acoustic equipment are shown in Fig. 1(a) and a schematic of the acoustic experiment setup is shown in Fig. 1(b).

The source was installed at 2 m from the bottom. The hydrophones were moored at 2 m, 4 m and 8 m from the sea bottom. The distance between the sound source and the mooring of hydrophones was approximately 122 m. The acoustic transect was close to the optode array installed at a water depth of 10 m (see Section 2.4).

The system used to transmit the probe signals comprised a portable acoustic source unit system (Saleiro, 2009) acting as a signal generator and signal amplifier, and the sound source Lubell LL916C underwater speaker. The sequence of probe signals was composed of a block of 3 groups of 10 chirps, each 3 s long, in three distinct frequency bands: low (400–800 Hz), medium (1500–3500 Hz) and high (6500–8500 Hz). The groups were separated by 2 s idle, within a group the chirps were 250 ms apart.

The frequency band (and to a lesser extent the source–receiver range) was decided taking into account the bands used by Hermand et al. (2000) and Hermand (2004). In the first reported experiment two low frequency signals in very close bands were used and no relevant differences between them were found. In the second experiment a signal with a larger band was used but the procedure to extract the acoustic variability was more complex and there was no apparent gain in using such a large band. The signals used in this work use a band similar to that used by Hermand (2004) but in three different (sub) bands to conclude about the signal band best suited to monitor O₂ production.

The signals were received at three SR-1 autonomous hydrophones from MarSensing (Soares et al., 2011), operating at a sampling frequency of 50781 Hz.

The acoustic experiment began with an engineering test from October 11 to October 14 devoted to preliminary data acquisition to determine the experimental setup, including the equipment and the transmitted signals (frequency bands, repetition rate, and number of signals in a block).

The data presented herein was gathered from October 16 to 18, covering almost two diel cycles. The hydrophones were recovered for maintenance at the middle of the period. Only one of the hydrophones

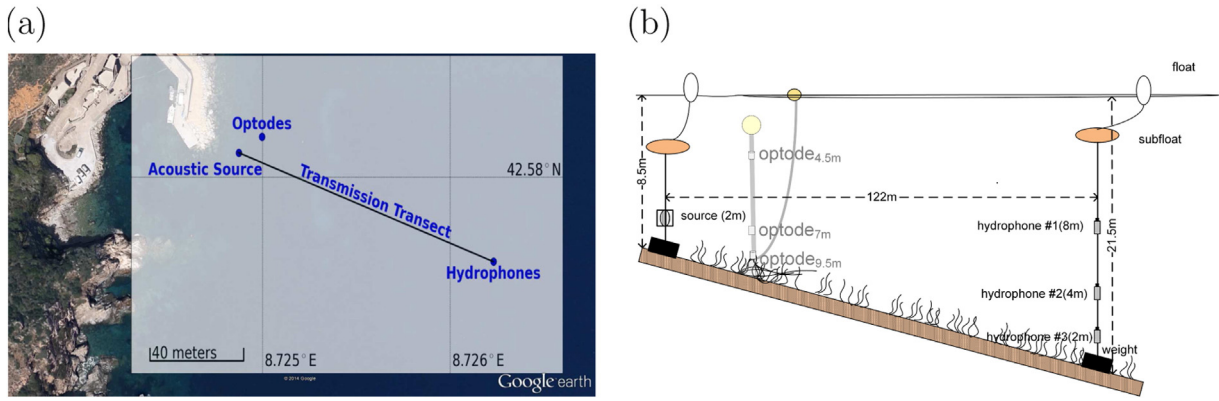


Fig. 1. Experimental setup: location of the source, hydrophone and optode moorings in the Bay of la Revellata (a) and schematic of the moorings (b). The values in brackets represent height from the seafloor.

has a battery pack sufficient to perform data acquisition repeatedly every 5 min during a period of 24-h. The data presented here is mainly from this hydrophone, that was positioned 4 m from the bottom. The hydrophones positioned at 2 and 4 m from the bottom acquired data at night to day and day to night transitions respectively. Although limited, the data from these hydrophones give some insight about the variability of the acoustic signal along the water column.

2.3. Environmental measurements

Acoustic propagation depends on a variety of environmental parameters (temperature, salinity, wind speed, wave height, and tide and source–receiver displacement) besides O₂ bubbles concentration. It is of paramount importance for acoustic signal analysis to acquire and take into account such data. During the experiment various sets of environmental data were gathered simultaneously with the acoustic transmissions.

Temperature and salinity profiles were acquired by a Conductivity, Temperature, and Depth (CTD) Sea-Bird SBE19, twice a day, at two locations: close to the receivers and at middle range between the source and the receiver. Sound speed profiles were computed from CTD data using the empirical approximation by Mackenzie (1981). In addition a temperature–pressure sensor (HOBO U20 Data logger) measuring the instantaneous temperature and source depth (1 sample/min) was collocated with the acoustic source.

Wind speed and direction were recorded in a meteorological station installed on the top of a STARESO station building at 11.8 m height at a distance of about 100 m from the source mooring.

2.4. Irradiance and dissolved O₂

Irradiance was measured at the surface and at 3 and 20 m depth. Oxygen saturation levels were obtained from O₂ measurements by an array of three Aanderaa O₂ optodes (3835) moored over the *P. oceanica* meadow at a water depth of 10 m, nearby the sound source (Fig. 1(a)). Oxygen concentrations were computed from O₂ saturation level, seawater temperature, and salinity (Champenois and Borges, 2012). The optodes acquired data hourly at 4.5, 7.0 and 9.5 m depth above the meadow as part of a permanent mooring installed in August 2006.

3. Acoustic data processing

Physical, chemical and biological processes in the sea give rise to perturbations of sound propagation. Methods to infer parameters of oceanic processes from sound waveforms were first proposed in the context of Ocean Acoustic Tomography by Munk et al. (1995). Next

are summarized methods that were used in the present work to represent and analyze the acoustic signature (perturbation of the acoustic signal) due to O₂ production by photosynthesis.

3.1. Arrival pattern

In a shallow water environment the waveform received by a hydrophone from a faraway source is the sum of the various echoes (signal replicas) traveling along the various paths. According to this simplified model, a single echo is characterized by its path, strength (amplitude) and delay. If $s(t)$ is the emitted signal, then the received waveform $y(t)$ is given by

$$y(t) = \sum_{n=1}^N a_n s(t - \tau_n) + n(t) \quad (1)$$

where N is the number of echoes, a_n and τ_n are the n -th echo strength and delay, respectively, and $n(t)$ is an additive random noise, uncorrelated with the signal, which encompasses various noise sources such as ambient and electronic noise. The set of parameters N , a_n , τ_n characterizes the propagation environment and may be used as indicators of environmental variability.

Pulse compression is a widely used procedure in underwater acoustics to identify the various echoes on the received waveform $y(t)$ (Munk et al., 1995). Pulse compression proceeds by cross-correlating the received signal $y(t)$ with the emitted signal $s(t)$ which, for random signals (due to the noise $n(t)$), is defined as

$$R_{ys}(\tau) = E \left[\int_T y(t) s(t - \tau) dt \right], \quad (2)$$

where $E[\]$ denotes mathematical expectation and T is a convenient time interval for integration. In practice mathematical expectation is replaced by averaging over a finite number of time intervals (transmissions). Therefore using Eqs. (1) and (2) an estimate of the cross-correlation function (pulse compression output) can be written as

$$\begin{aligned} \hat{R}_{ys}(\tau) &= \frac{1}{K} \sum_{k=1}^K \left[\int_{(k-1)T}^{kT} \sum_{n=1}^N a_n s(t - \tau_n) s(t - \tau) + n(t) s(t - \tau) dt \right] \\ &= \sum_{n=1}^N \left[\frac{1}{K} \sum_{k=1}^K \int_{(k-1)T}^{kT} a_n s(t - \tau_n) s(t - \tau) + n(t) s(t - \tau) dt \right] \\ &= \sum_{n=1}^N a_n \hat{R}_{ss}(\tau - \tau_n) \end{aligned} \quad (3)$$

where K is the number of time intervals, the uncorrelation between signal and noise was used to eliminate the second term on the right hand side and $\hat{R}_{ss}(\tau)$ is the estimate of the autocorrelation function of the emitted signal $s(t)$. Some authors use the term reduced time for delay variable τ . As per Eq. (3) if R_{ss} is a “peaky function”, the pulse compression output allows to identify N successive peaks with relative amplitudes a_n and delayed by τ_n , which are the variables that characterize the channel through which the signal $s(t)$ propagated. Here, “peaky function” means that its time duration is small compared to the shortest interval between two successive arrivals. Large bandwidth chirp signals, such as those used in this experiment, have this property. When plotting, the envelope of $\hat{R}_{ys}(\tau)$ known as the arrival pattern is rather used than the pulse compressed output.

3.2. Frequency response of acoustic channel

Assuming a high signal to noise ratio, the random noise component of the received waveform can be neglected. Therefore, the frequency domain counterpart of Eq. (2) is given by

$$S_{ys}(f) = |H(f)|^2 S(f) \quad (4)$$

where $S(f)$ is the power spectral density of the emitted signal, $S_{ys}(f)$ is the cross power spectral density of the received and the emitted signal, and $|H(f)|^2$ is the magnitude squared of the frequency response of the acoustic channel. It has been established that the variability of the acoustic channel has an acoustic signature that is frequency dependent (Medwin and Clay, 1998). Analyzing the channel frequency response dependence on photosynthetic activity provides a guideline for selection of the optimal frequency band of the probe signal.

Taking into account Eq. (4), one can estimate the squared magnitude of the frequency response of the acoustic channel, $\hat{H}(f)$, by

$$|\hat{H}(f)|^2 = \frac{|\hat{S}_{ys}(f)|}{|\hat{S}(f)|} \quad (5)$$

where $\hat{S}_{ys}(f)$ and $\hat{S}(f)$ are the estimates of $S_{ys}(f)$ and $S(f)$, respectively. In practice, when a reference hydrophone is not available (like in the present work) the power spectral density of emitted signal becomes equal to the sound source frequency response (as given by technical specifications), up to a constant factor.

3.2.1. Received energy

It was shown (Hermand et al., 2000) that the acoustic signal is highly attenuated during the active period of photosynthesis with the perturbation of the received energy acting as a proxy for O_2 production. Since we are interested in the variation of the received energy rather than in its absolute value, the energy of the pulse compressed signal

$$\hat{E} = \int |\hat{R}_{ys}(\tau)|^2 d\tau \quad (6)$$

can be used. It is assumed that the energy of the transmitted signal is kept constant with time. The period of integration is bounded by the arrival time of earlier and later echoes.

3.3. Acoustic- O_2 mapping

In order to use acoustic based methods as a tool for estimating the seagrass O_2 production at the ecosystem level, it is necessary to map the acoustic measurements into meaningful ecosystem parameters like net ecosystem production, which can be derived from O_2 measurements (Champenois and Borges, 2012). Roberts and Caperon (1986) and Roberts and Moriarty (1987) showed a linear relationship between dissolved O_2 and bubbles released into the water column by seagrasses.

Therefore, in this work we applied a linear regression model at the 5% significance level between the variability of the energy of the received acoustic signal and the variability of the dissolved O_2 measured at the array of the 3 optodes. The linear regression model was applied to individual optode measurements and to water column (10 m) average value. The average O_2 concentration was obtained considering 5 layers (Champenois and Borges, 2012): (1) 10.0 to 9.0 m; (2) 9.0 to 7.5 m; (3) 7.5 to 6.5 m; (4) 6.5 m to 5.0 m; and (5) 5.0 m to surface. The O_2 concentrations in layers 1, 3 and 5 are given by the actual O_2 optode measurements. The concentration considered in layers 2 and 4 are obtained by the average of the two nearest optode measurements. The whole water column average concentration Q_{avg} is then given as

$$Q_{avg} = (6.75Q_{4.5m} + 2.5Q_{7m} + 1.75Q_{9.5m})/10, \quad (7)$$

where $Q_{4.5m}$, Q_{7m} and $Q_{9.5m}$ represent the O_2 optode measurements at 4.5 m, 7 m and 9.5 m depth, respectively.

4. Results

4.1. Environmental measurements

Fig. 2 presents a summary of the environmental data set gathered from October 16 to October 18. The temperature and salinity profiles (Fig. 2(a) and (b)) acquired by a CTD, twice a day, along the transect were constant with depth, giving rise to slightly upward refracting sound speed profiles (Fig. 2(c)). The presented profiles show no significant spatial variation along the source–receiver transect. The sound speed estimated from CTD data, increased about 5 m/s during the period, because of a quasi-monotonic increase of temperature as seen in the temperature sensor installed at the source (Fig. 2(d)).

Fig. 2(e) shows the instantaneous measurements of the source depth. It is clear from the figure that the source depth is modulated by the surface tide and surface agitation, with an amplitude below 0.5 m. The dispersion of the instantaneous source depth values decreased with time because of the sea becoming calmer.

The wind speed presented in Fig. 2(f) decreased significantly after noon of May 16 from 7 m/s to 1 m/s in less than 6 h. During the next 24-hour period, the wind speed was lower than 4 m/s. The following night the wind increased, reaching 9 m/s at noon of October 18.

4.2. Irradiance and dissolved O_2

Fig. 3 shows the variation with time obtained at various depths of irradiance (a), dissolved O_2 concentration (b) and O_2 saturation level (c). The trend of peaks and troughs are related to the diel photosynthetic cycle. The higher values of dissolved O_2 were observed at 9.5 m, i.e., just above the canopy. One can remark that the highest peaks of dissolved O_2 on October 18, particularly at the deepest and shallowest sensors, are in line with the highest irradiance levels, most visible at 3 m depth. O_2 super-saturation (relative to atmospheric equilibrium) were observed during the whole period, which is the normal situation from spring to fall at this site (Champenois and Borges, 2012), and has also been noted in other studies (Wilson et al., 2012). When super-saturation occurs, free gas bubbles affect sound propagation (Medwin and Clay, 1998).

Therefore, a high correlation between the variability of the dissolved O_2 and the variability of the acoustic signal is expected. This will be discussed later.

4.3. Arrival patterns

Fig. 4 shows the arrival patterns from October 16, 16:00 to October 18, 15:00 acquired at the hydrophone 4 m above the bottom. The gap in the data occurred during hydrophone maintenance. The arrival patterns revealed a clear difference between the strength of the echoes

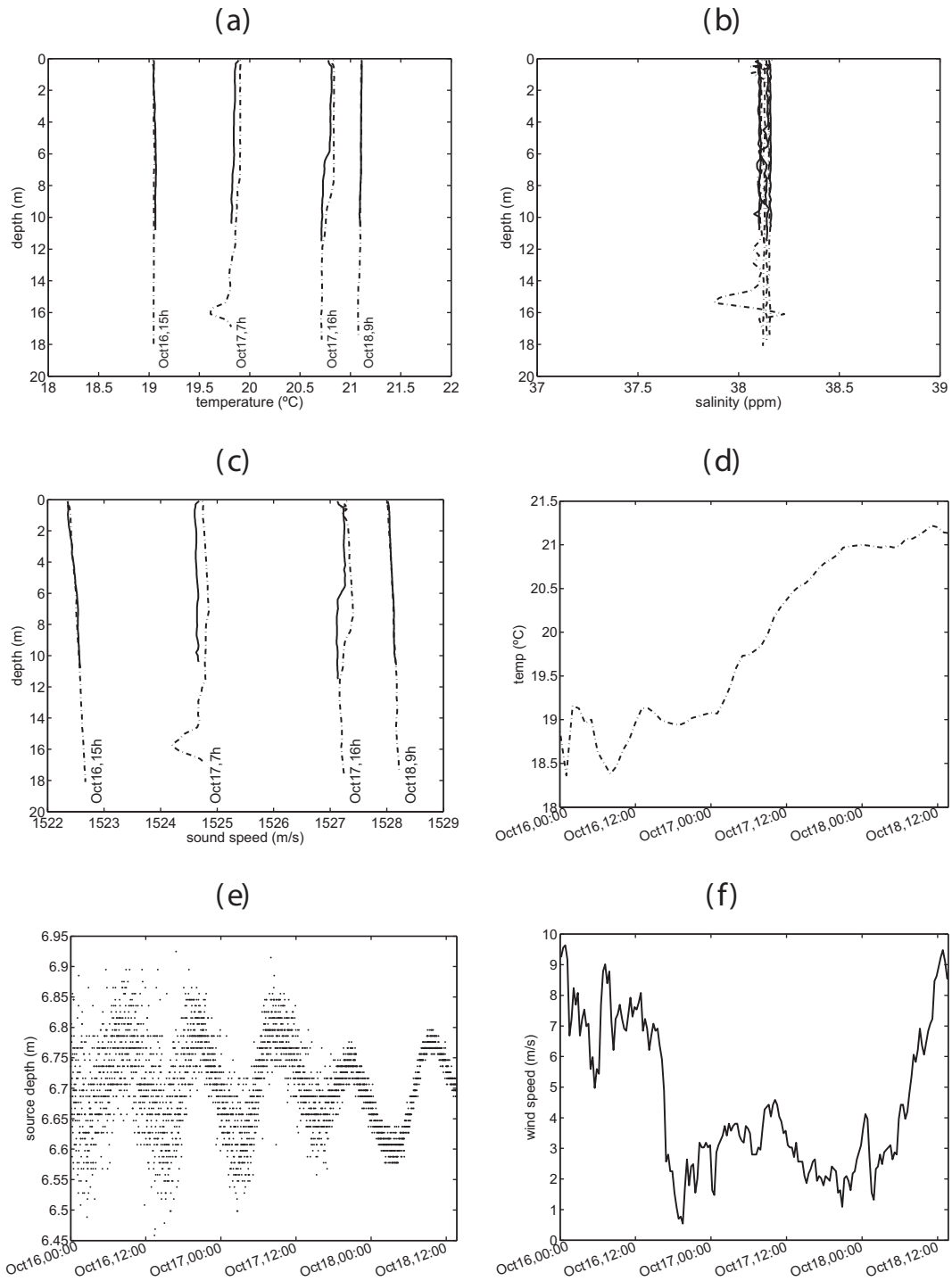


Fig. 2. Environmental data measured in the Bay of la Revellata from October 16, 00:00 (GMT) to October 18, 2011, 12:00 (GMT): CTD temperature (a) salinity (b) and sound speed (c) profiles at the hydrophone mooring (dash-dotted line) and at a middle location in the transect (solid line), temperature at the source depth (d), source depth (e) and wind speed at the top of a STARESO building (f).

during the day (lower amplitudes) and night period (higher amplitudes) for low 400–800 Hz and medium 1500–3500 Hz frequency signals, respectively Fig. 4(a) and Fig. 4(b). For high frequency signals this pattern was not evident, Fig. 4(c). At sunrise (5:00 (GMT)), there is an abrupt change (decay of echo strength) in the arrival patterns that can be ascribed to the onset of the photosynthesis. Also, the arrival patterns show a higher variability during the day period than during the night due to variability in O₂ production during the day.

The biological scattering due to fish schools and other organisms present in the seagrass meadow can also significantly contribute to the variability of the acoustic signal. During the experiment various fish schools were observed in the area by SCUBA divers. The planktivorous damselfish *Chromis chromis* and *Sarpa salpa* a macro-grazer of seagrass represent the most abundant fish schools within *P. oceanica* meadows. Previous studies conducted in the STARESO meadow did not suggest a visible correlation between the diel behaviors of *C. chromis* (Pinnegar

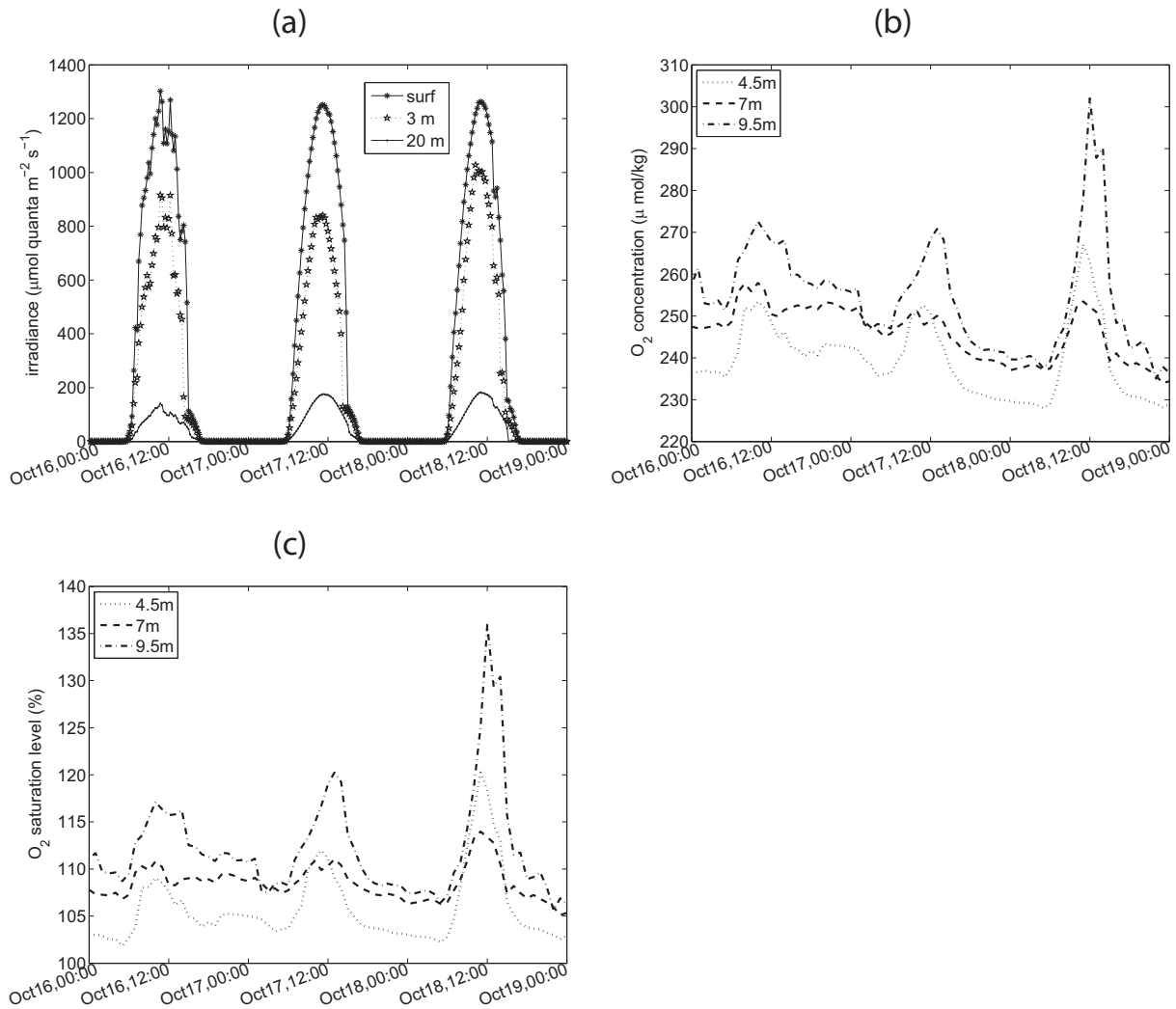


Fig. 3. Irradiance (a), dissolved O_2 concentration (b), and saturation level (c) at various depths over the *P. oceanica* meadow in the Bay of la Revellata from October 16, 2011, 00:00 (GMT) to October 18, 2011, 24:00 (GMT).

et al., 2007) and *S. salpa* (Jadot et al., 2006) schools and the variability of the acoustic signal observed in the present work. Nevertheless, this issue deserves attention in forthcoming experiments.

The average arrival patterns computed from transmissions between October 17, 16:00 and October 18, 15:00 are shown in Fig. 5, where the blue curve was computed from whole day transmissions, the red curve from the day period (after from 5:00 to 15:00) and the black curve from the night period (from 19:00 to 5:00). The logarithmic dB-scale used in the plots balances the amplitudes between the first (strong) arrivals and the latter (weak) arrivals. Due to a narrower effective bandwidth of low frequency signals their arrival patterns have lower resolution and several echoes are grouped in a single lobe (Fig. 5(a)).

In low frequency arrival patterns during the day period the attenuation is already visible in the first peak, but in medium frequency arrival patterns are particularly notable in latter ones (Fig. 5(b)). A similar pattern was observed in previous days.

In general, these results corroborate early findings by Hermand et al. (2000) and Hermand (2004), and suggest that arrival patterns from low and medium frequency signals can be used both as a proxy for photosynthesis and a basis for estimating oxygen production. On the other hand the results show that the high frequency signals are not suitable as a proxy for photosynthesis. Hereafter, the results and the discussion are focussed on low and medium frequency signals.

4.4. Channel frequency response

Fig. 6 shows the estimated frequency response of the acoustic channel in the low frequency and medium frequency bands for the period considered in Fig. 5.

The frequency response of the Lubell LL916C source varies considerably in the low frequency band, increasing almost linearly about 20 dB from 400 Hz to 800 Hz, therefore the procedure described in Section 3.2 was applied. In the medium frequency band the response of the source is nearly flat (the variation is less than 3 dB), therefore it was considered that the power density spectrum of the emitted signal is constant between 1500 and 3500 Hz.

In both signal bands, one can notice a remarkable difference between the frequency response of the channel during the day and night periods. Similarly with arrival patterns, there was an abrupt change in the frequency response at sunrise (5:00 GMT), and variability in the frequency response is higher during the day period than during the night.

These changes in the frequency response suggest a complex modal interference pattern due to a possible formation of a low sound speed channel close to the bottom during photosynthetic activity (Hermand et al., 2000). A similar pattern is observed in both frequency bands, where the dominant frequencies suffer a shift during the day. As expected, this shift is smaller for low frequency signals than medium frequency signals. In low frequency signals during day, one can notice a steeper decrease of energy.

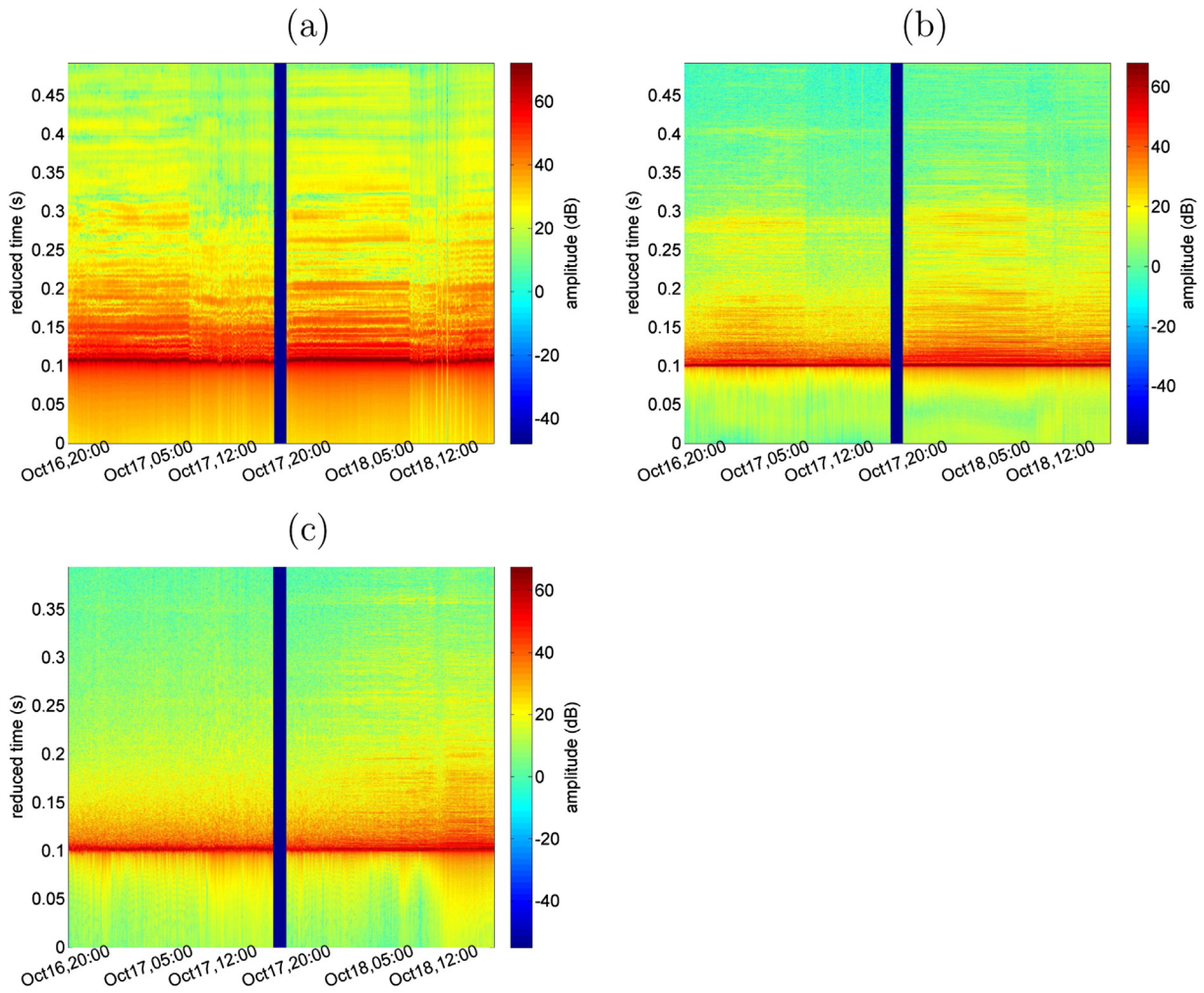


Fig. 4. Arrival patterns estimated using Eq. (3) from October 16, 16:00 (GMT) to October 18, 2011, 15:00 (GMT) for low frequency signals (400–800 Hz) (a), medium frequency signals (1500–3500 Hz) (b) and high frequency signals (6500–8500 Hz) (c), at hydrophone located 4 m above the bottom. Color represents the relative echoes strength.

4.5. Received energy

Fig. 7 presents the variation of the average of the received energy using Eq. (6), for the three frequency bands. The dots represent a single

value (corresponding to a block of transmissions), whereas the black lines represent a moving average corresponding to half-hour averaging time (6 blocks). As explained above, the data gap that occurred on the afternoon of October 17 is due to the recovery of the hydrophones for

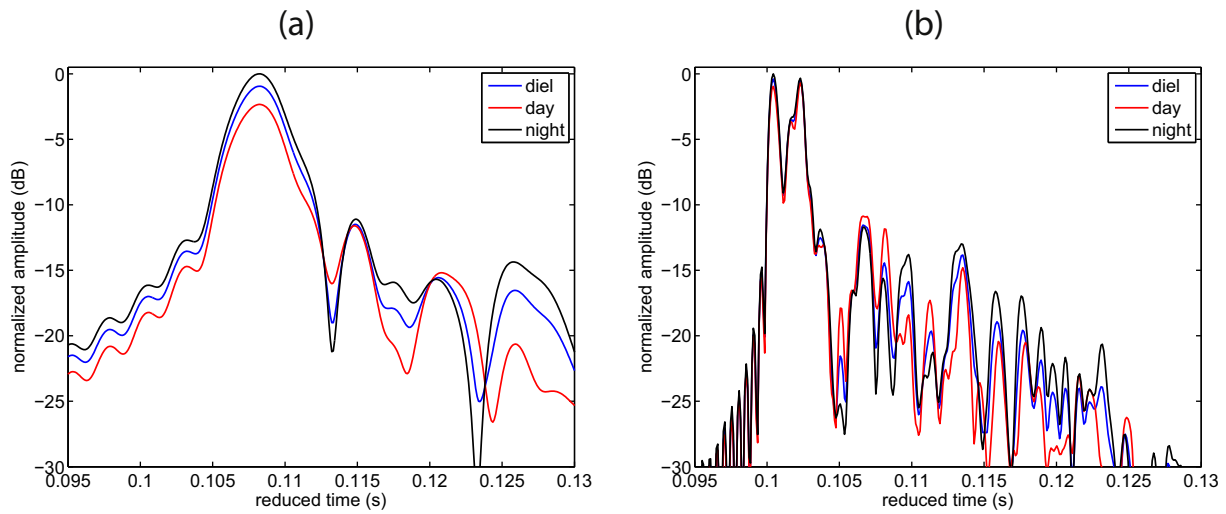


Fig. 5. Average arrival patterns from data acquired between October 17, 16:00 (GMT) and October 18, 15:00 (GMT) every 5 min at hydrophone 4 m from the bottom: low frequency signals (400–800 Hz) (a), medium frequency signals (1500–3500 Hz) (b). Blue line – whole day transmissions, red line – day transmissions (from 5:00 to 15:00), and black line – night transmissions (from 19:00 to 5:00). (For interpretation of the references to color in this figure, the reader is referred to the web version of this article.)

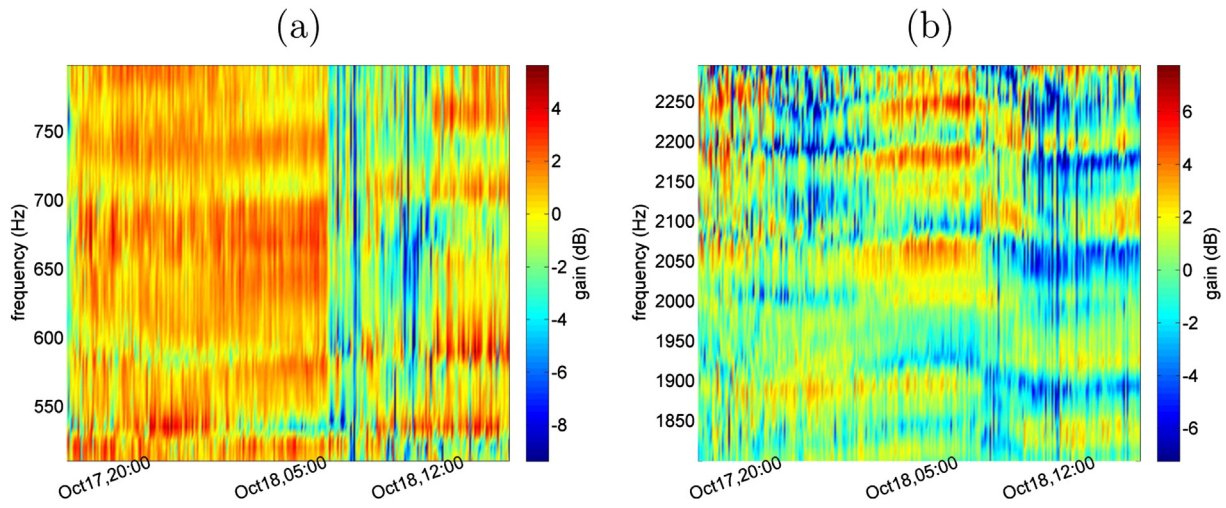


Fig. 6. Estimated frequency response of the acoustic channel using Eq. (4) from October 17,2011, 16:00 (GMT) to October 18, 2011, 15:00 (GMT) at hydrophone located 4 m above the bottom: low frequency band (400–800 Hz) (a), and medium frequency band (1500–3500 Hz) (b).

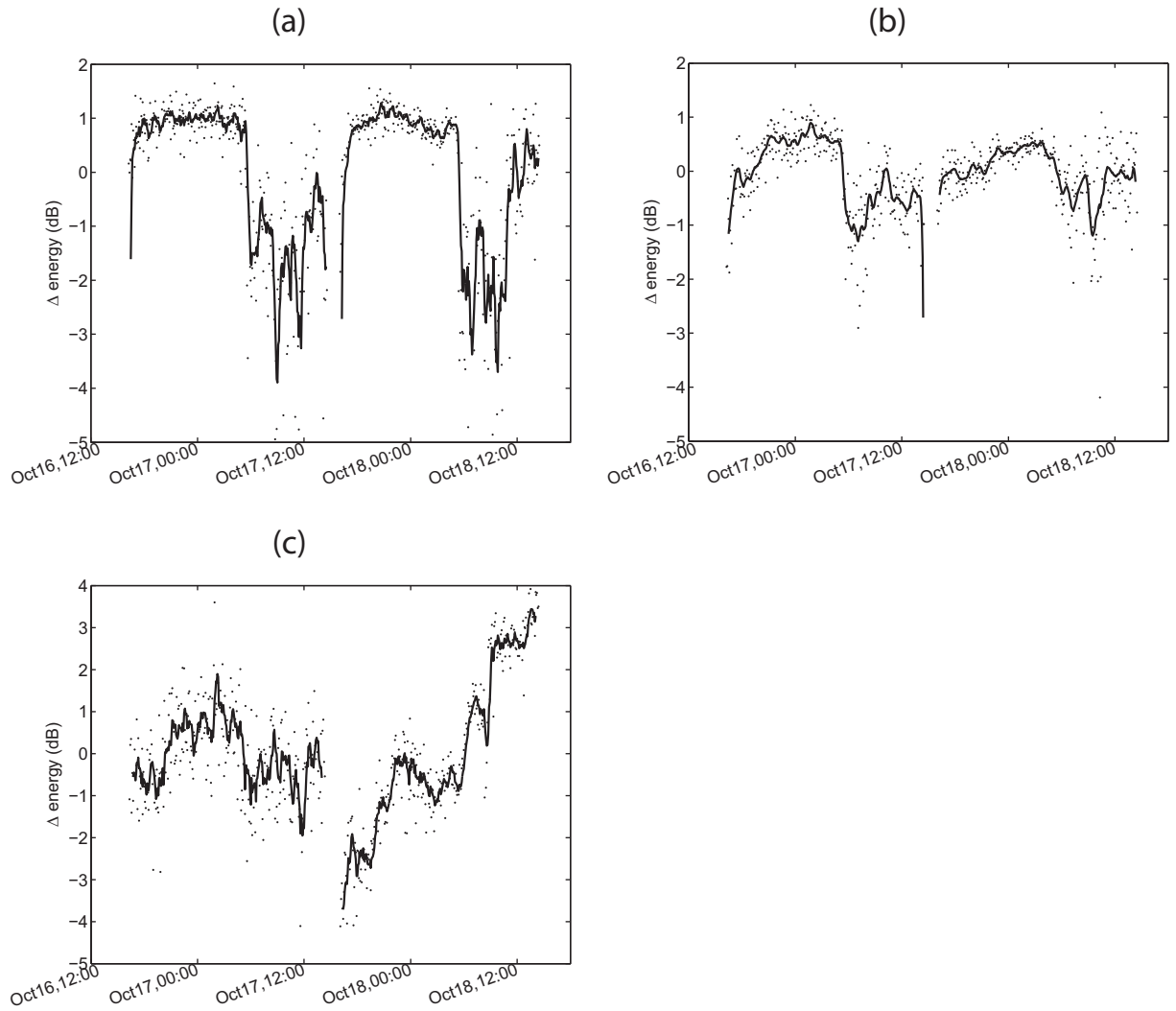


Fig. 7. Variability of the received acoustic energy from October 16, 2011, 16:00 (GMT) to October 18, 2011, 15:00 (GMT) for low frequency signals (400–800 Hz) (a), medium frequency signals (1500–3500 Hz) (b) and high frequency signals (6500–8500 Hz) (c) at hydrophone at 4 m above the bottom. Instantaneous (block) values are represented by dots and half-hour moving average values by solid line.

data downloading and battery replacement. Due to this recovery and redeployment, the conditions of the experiment have most likely changed slightly, because it was not guaranteed that the hydrophone was redeployed exactly at the previous position. An average change of 3 dB was found for the low frequency signals, while the change for medium frequency signals was 1.5 dB.

The energy of the received signal along time is a simple method to quantify the time variability of the acoustic signal. As for the arrival patterns and frequency response of the acoustic channel it is assumed that the source strength does not vary along time. This was achieved by keeping the gain of the source system constant during transmissions. However, when the hydrophones were recovered, the source was switched off, and we could not be certain that the gain of the source system did not change slightly when it was turned on again.

Despite these technical issues one can remark that the patterns of the curves for low and medium frequency signals are similar in both diel periods and suggest that the received energy is highly correlated with photosynthetic activity.

For the high frequency signals (Fig. 7(c)) the pattern in the first diel period is in-line with the patterns of the low and medium frequency signals showing a correlation between the received energy and the photosynthetic activity, but in the second diel period, the energy of the received signal unexpectedly increased during the day period.

The hydrophones at depths 2 and 8 m above the bottom acquired data only during the night to day and day to night transition periods, respectively. During these periods one can notice the similarity between the curves at the different depths for low and medium frequency signals as shown in Fig. 8. These findings indicate that the depth of the hydrophone is not a stringent constraint of the acoustic system setup.

4.6. Acoustic energy – dissolved O₂ correlation

The results presented so far suggest a correlation between the diel perturbation of the acoustic signal transmitted through the *P. oceanica* meadow and photosynthetic O₂ production. Very often, the primary production of a meadow is assessed using dissolved O₂ measured by methods such as Winkler titrations, Clark-type electrodes or optodes, which are not capable of quantifying the gas bubbles, leading to an underestimation of system primary production. The acoustic signature is driven by bubbling and the gas in aerenchyma, therefore combining

acoustic and chemical techniques might allow the development of a more robust and accurate methodology for estimating in-situ productivity of seagrass meadows (Wilson et al., 2012).

Roberts and Caperon (1986) and Roberts and Moriarty (1987) showed a linear relationship between gases discharged from the lacunae and oxygen released into the water column. How can we best compare the perturbation measured in the acoustic signal with the dissolved O₂ measurements? In this work we pair the perturbations of the acoustic energy with the perturbations of the dissolved O₂ measured by the array of 3 optodes. Fig. 9 shows the half-hour moving average of the acoustic energy (in dB) measured by the hydrophone 4 m from the bottom represented by the solid curve, superimposed in curves representing the perturbations of the O₂ concentrations calculated from data presented in Fig. 3(b), where the dotted line corresponds to the optode at 4.5 m, the dashed line to the optode at 7.0 m and the dash-dotted line to the optode at 9.5 m. These data are related to the second acquisition period in Fig. 7. There is a negative correlation between the perturbation of the acoustic energy and the perturbation of the O₂ concentration (reversed y axis on the right hand side of Fig. 9). At sunrise, the change in acoustic signal occurred faster than the change in O₂ concentration, in particular for the low frequency signal. Similar pattern was described by Wilson et al. (2012). During the day period the peak (minimum) of acoustic energy perturbation in both signal bands is observed at the peak (maximum) of the O₂ perturbation at 9.5 m optode. On the other hand, the O₂ perturbation along the day period is smooth, but the perturbation of the acoustic energy both for low and medium frequency signals shows several oscillations.

In order to evaluate the map between the perturbation in O₂, δO_2 , at the various optodes and the perturbation in the acoustic energy ΔE as a linear model

$$\delta O_2 = m\Delta E + b, \quad (8)$$

a least squares regression at 5% confidence level was applied. The sampling rate of the acoustic data is 12 samples/h whereas the sampling rate of the optode data is 1 sample/h, thus the value considered for energy perturbation was obtained by linear interpolation of the samples before and after the optode sample. Since the perturbation in the acoustic signal integrates contributions from the whole water column, we also estimated the parameters of fitting a linear model between the acoustic perturbation and the water column average O₂ concentration.

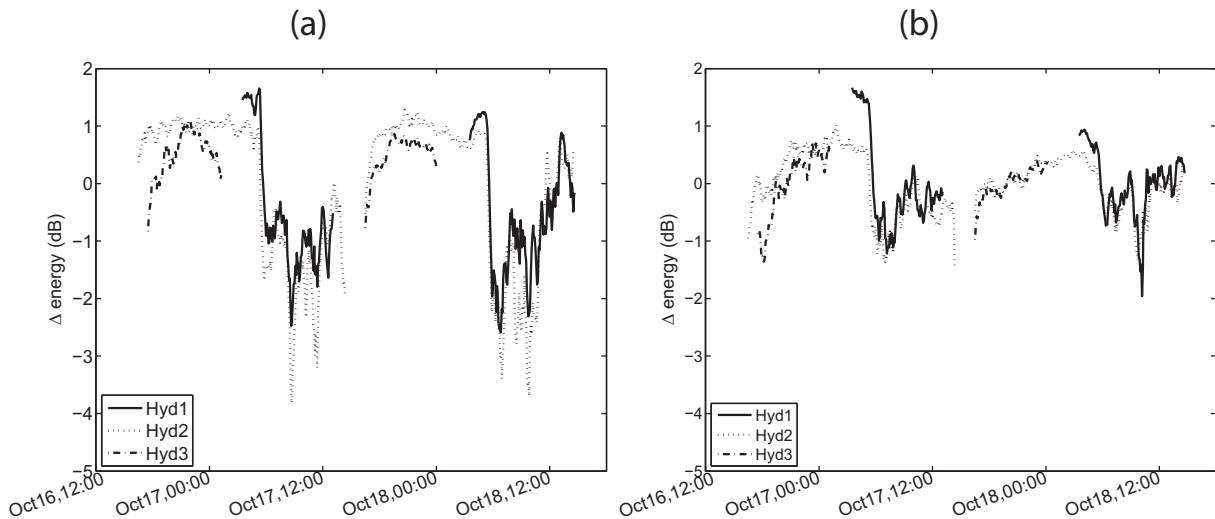


Fig. 8. Received acoustic energy (average) at depths 2 m (Hyd3), 4 m (Hyd2) and 8 m (Hyd1) above the bottom from October 16, 2011, 16:00 (GMT) to October 18, 2011, 15:00 (GMT) for low frequency signals (400–800 Hz) (a) and medium frequency signals (1500–3500 Hz) (b). The hydrophone Hyd1 acquired data at night to day transitions (solid line), the hydrophone Hyd3 (dash-dotted line) acquired at day to night transitions. The curves for hydrophone Hyd2 (dotted line) are the averages presented in Fig. 7(a) and (b) for low and medium frequency signals respectively.

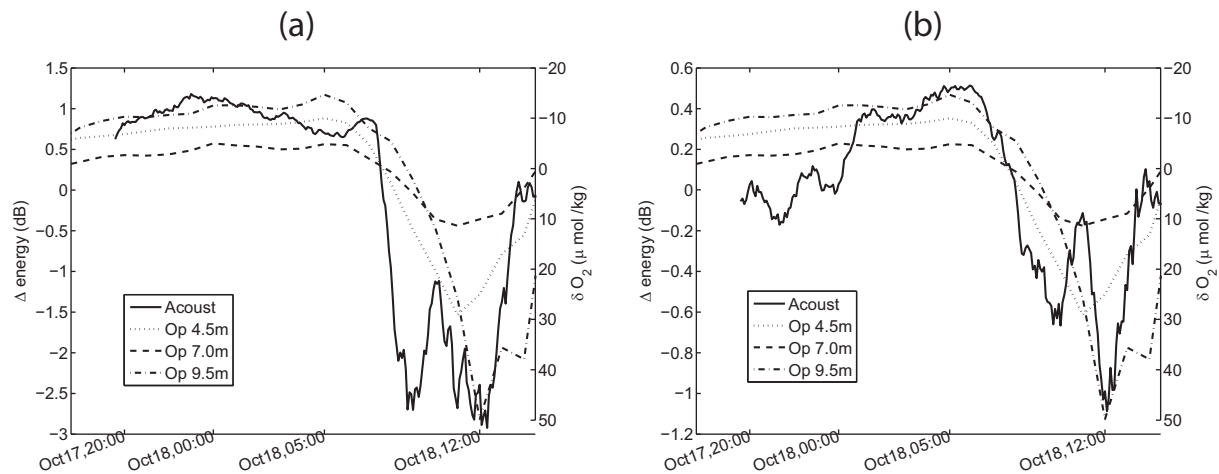


Fig. 9. Comparison between O_2 changes measured by the optodes at various depths (4.5 m dotted curve, 7 m dashed curve, 9.5 m dash-dotted curve) and the variability of the half-hour moving averaged energy of the acoustic signal at hydrophone 4 m above the bottom (solid line), from October 17, 2011, 16:00 (GMT) to October 18, 2011, 15:00 (GMT): low frequency signals (400–800 Hz) (a), medium frequency signals (1500–3500 Hz) (b).

It is important to stress the different nature of the measurements: whereas dissolved O_2 are point measurements, and the acoustic measurements represent integral measurements.

The estimated model parameters and statistics are presented in Table 1, whereas Fig. 10 shows the scatter plot and the regression lines.

The statistical values ($P < 0.001$) suggest that the linear model can be accepted. Coefficients of determination (correlation – R^2) greater than 0.6 were found at optode depth 7.0 m for both signal bands corresponding to the lowest error variance. Conversely, the larger error variance and the lowest coefficient of determination were found for the optode at 9.5 m. It is clear that the most reliable correlation is between the perturbation of acoustic energy and the perturbation of the O_2 concentration at 7.0 m depth. As expected the linear model parameters found for the average concentration reflect the weight of the different optodes used in the computation of the average value.

5. Discussion

This work builds on previous efforts by Hermand et al. (2000) and Hermand (2004) using acoustic signals to derive O_2 dynamics and ecosystem metabolism in seagrass meadows. Our results corroborate the general pattern of the *P. oceanica* photosynthetic activity signature in the acoustic signal reported in previous studies, but we also show that the photosynthetic signature at sunrise appears earlier in the acoustic signal than in O_2 measurements by optodes (Fig. 9). This behavior could be related to the pressurization of the aerenchyma at sunrise (Borum et al., 2006), and it might suggest that photosynthetic activity affects the acoustic signal even in the absence of conditions that allow

the release of free bubbles. The validation of such a hypothesis would require a further experiment to be conducted in lower productivity conditions. The present work also investigated the influence of the frequency band of the probe signal on the acoustic signature, showing that the slope of the change of the acoustic signal is related to the frequency band and that at the highest signal frequency band considered the simple proposed method failed (see a possible explanation below). The frequency band is a key point for the implementation of a simple and robust monitoring system. The procedure used by Hermand (2004) to extract the acoustic signature from the band 0.2 kHz–16 kHz, which required the identification and extraction of a group of arrivals from the arrival pattern, is more complex and sensitive to the geometry of the experiment (water depth, source–receiver range and depth) than the procedures used in the present work and in Hermand et al. (2000), where lower frequencies (<3.5 kHz) and shorter bands were used. On the other hand, the autonomy and the size of the acoustic system are directly related to the frequencies used. An acoustic monitoring system designed to operate at frequencies (1.5 kHz–3.5 kHz) such as that used in this study has certain advantages. It could be smaller and have a larger autonomy than systems operating at lower frequencies, yet allowing a simple procedure to track the O_2 variability.

The factors that influence the acoustic response of a seagrass are not well established, but it is considered that free gas bubbles emanating from the plants and the pressurization of the aerenchyma by non-dissolved gas produced during photosynthesis are the most relevant. Both factors influence the compressibility thus the effective sound speed of the medium. The compressibility κ is related to sound speed c by

$$c = \sqrt{1/(\kappa\rho)}, \quad (9)$$

where ρ is the density. The free gas bubbles increase the acoustic compressibility of the seawater (Hermand, 2004), whereas an increase of internal pressurization should give rise to a decrease of acoustic compressibility. However, leaf morphology and the total biomass also influence acoustic compressibility of the seagrass and various patterns were observed among seagrasses (Wilson and Dunton, 2009); (Wilson et al., 2010, 2012). Until now, it was not possible to find a model that allows to quantitatively describe the acoustic response of seagrasses. However, the particular behavior of a certain seagrass species could be related to the dominant effect for that species. In the case of *P. oceanica* the major driving factor should be the free gas bubbles emanating from the plants, which increases the compressibility of the seawater, therefore a decrease of the effective sound speed.

Table 1

Statistical comparison of linear regression coefficients (m-slope, b-intersect) estimated from acoustic energy perturbation onto O_2 perturbation at various depths and water column average value (avg val) given by Eq. (7).

	m	b	R^2	F-value	p-Value	Error variance
<i>Low frequency</i>						
Opt. 4.5 m	–7.9	0.0	0.73	51.0	<0.0001	47.9
Opt. 7.0 m	–3.4	0.0	0.70	44.7	<0.0001	10.1
Opt. 9.5 m	–9.0	0.0	0.41	13.0	0.002	243.9
Avg val	–7.8	0.0	0.66	36.3	<0.0001	62.6
<i>Medium frequency</i>						
Opt. 4.5 m	–26.3	0.0	0.55	22.8	0.0001	80.2
Opt. 7.0 m	–12.1	0.0	0.60	28.5	<0.0001	13.5
Opt. 9.5 m	–38.1	0.0	0.49	18.4	0.0004	208.24
Avg val	–27.4	0.0	0.56	24.5	<0.0001	81.7

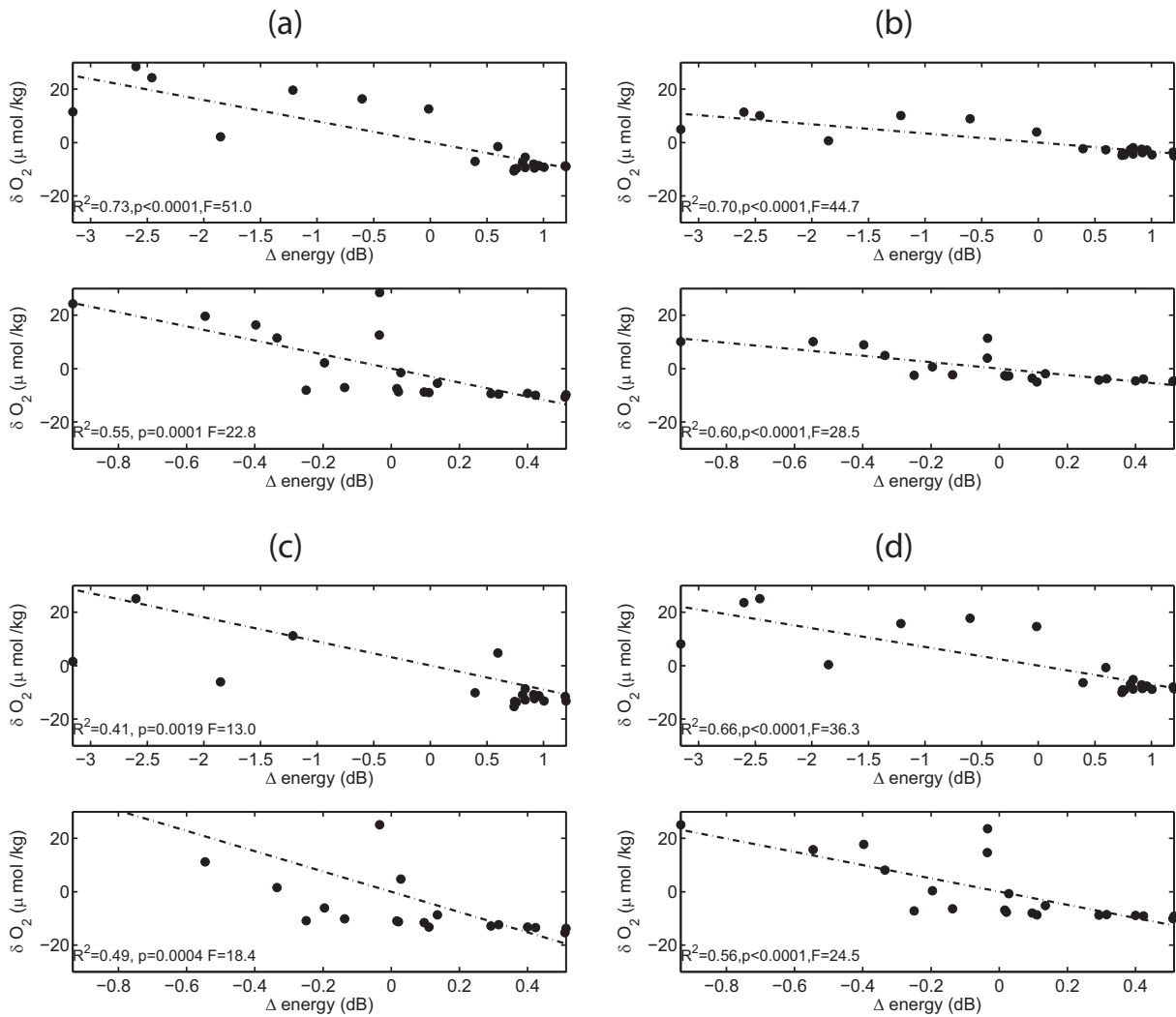


Fig. 10. Linear regression between acoustic energy (low frequency band – upper subplots, medium frequency band – lower subplots) and dissolved O₂ perturbations measured by optode at 4.5 m (a), 7 m (b), 9.5 m (c) depth and water column average value given by Eq. (7) (d). The legend represents the R² statistic, the p value and the F statistic for the linear model.

For high frequency signals close to the resonance frequencies of the bubbles, high attenuation and dispersion of sound are expected. The resonance frequency of the bubbles depends mainly on the bubble radius. To the best of our knowledge the bubble radius of *P. oceanica* is not available in the literature, but Wilson et al. (2012) have found a mean radius around 0.5 mm of bubbles released by *S. filiforme* and *H. wrightii*. Using the simplified expression for the resonance frequency f_r of a spherical air bubble of radius a at depth z (Medwin and Clay, 1998)

$$f_r = \frac{3.25\sqrt{1 + 0.1z}}{a} \quad (10)$$

we obtain a resonance frequency around 10 kHz ($z = 10$ m). In case that the radius of the bubbles released by the *P. oceanica* in the present experiment was similar, one might expect a significant attenuation of the high frequency signals used. However the results presented in Fig. 7(c), where the received energy increased during photosynthetic activity of the plants suggests that the resonance frequency is not close to 10 kHz, the bubble radius is presumably smaller, and the resonance frequency is higher.

For low frequency signals, well below the resonance frequency, sound propagation is mainly affected by the decrease of effective sound speed, which is proportional to bubble concentration. Under significant

bubble concentration the sound speed value obtained from CTD measurements based in temperature, salinity and depth alone (like in Fig. 2(c)) is overestimated (Medwin and Clay, 1998). An increase of free bubbles in the seagrass layer gives rise to a low sound speed channel close to the bottom that induces refraction of the sound and a number of bottom interactions. In long range propagation, the seagrass layer increases the attenuation of the transmitted signal that is proportional to the bubble concentration. An increase in attenuation produces a decrease in energy of the received signal, thus the variability of the energy of the received signal is highly correlated with the bubbles produced by photosynthesis. This pattern was clearly verified for the energy received from low frequency and medium frequency signals (Fig. 7) and is highly correlated with the measurements of dissolved O₂ (Fig. 9).

The contribution of dissolved O₂ for the propagation of sound is appreciable when compared with the contribution of gas bubbles, but it is supposed to be positively correlated with gas bubbles (Wilson et al., 2012). Therefore, the changes in the acoustic signal can potentially be used as a proxy of meadow production for *P. oceanica* and other seagrasses with similar acoustic response. Despite the high correlation of circadian changes of the acoustic signal with other photosynthesis proxies like dissolved oxygen or PAR, there are particular issues that should be considered. At sunrise, with the onset of photosynthesis, the change of the acoustic signal occurs faster than the change of the dissolved O₂ measured at the various depths (Fig. 9). Such behavior was

also reported in previous works and suggests a rapid build-up of oxygen at sunrise (Hermand, 2004).

Since the acoustic signal samples the seagrass directly, this transient can be seen instantaneously by acoustics, but only after oxygen diffusion to the seawater by the optodes, therefore with some delay. However, one can see that the slope of the change varies also with the frequency band of the acoustic signal appearing earlier (faster) in the low frequency signal (Fig. 9(a)) than in the medium frequency signal (Fig. 9(b)). The day–night variability in medium frequency signals is more visible in latter echoes (Fig. 5(b)), therefore it is related to higher order modes, which have a low group velocity. But in the low frequency signals the major day–night variability occurs in the first echoes (Fig. 5(a)), therefore it is related to lower order modes, which have high group velocity. Moreover, the frequency cut-off effect of the waveguide can be seen at low frequencies, where frequencies below 600 Hz are highly attenuated and a drop off of energy is clearly seen at various occasions during daytime. This can be attributed to (lower) modes cut-off conditions appearing during photosynthesis. The combination of these factors leads to a non-linear jump in low-frequency, where a small increase in O₂ concentration gives rise to a large drop in the energy, but a further increase of the oxygen concentration has a smaller effect on the additional energy decrease. In both frequency bands the instantaneous variability of the acoustic signal is higher during the day than during the night with several “peaks and valleys” (Figs. 7 and 9). This suggests the occurrence of transient flows in the lacunar system of the seagrasses. These instantaneous perturbations affect the acoustic signal which traverse the seagrasses, but due to the indirect nature of measurement and the filtering effect of seawater cannot be detected by optodes, which show a smooth variation of the dissolved oxygen with the photosynthesis.

Despite the different nature and time scale of sampling performed by the acoustic signal and the optodes the mapping between measurements is well fitted by a linear model (Table 1 and Fig. 10). The comparison of the regression curves for low frequency and medium frequency bands in Fig. 10 shows that the curves related to the optode at 4.5 m and 7.0 m depth have the same slope if a normalized energy perturbation is considered (that is the energy perturbation is expressed relative to the minimum and maximum values for the given signal band). A question arises: does the slope of the linear regression remain constant over several days? In the present experiment, the hydrophones were recovered daily by changing their position, therefore this question cannot be definitely answered.

In this paper the metric used to quantify the perturbation of the acoustic channel due to photosynthesis was the energy perturbation. This very simple method gave meaningful results in low and medium frequency bands. The arrival patterns showed that echoes most affected by photosynthesis varied depending on the frequency band considered. Therefore methods that select portions of the arrival patterns according to the band of the signal are likely to be more robust and would effectively filter out perturbations that are linked to non-photosynthetic processes. Similarly, the perturbation of the acoustic signal can be estimated from the modal interference patterns present in the spectrogram. These methods were proven to be efficient in estimating the sea bottom parameters (number of bottom layers and their sound speed, density and attenuation) using a single hydrophone (Bonnell et al., 2013).

6. Conclusions

This work shows that photosynthesis significantly affects acoustic propagation below 10 kHz through a *P. oceanica* meadow. Signals in three different frequency bands were analyzed. For the lower band considered (400–800 Hz), which includes the cutoff frequency for the waveguide, the attenuation is remarkable for the earlier echoes arriving at the receiver or conversely for the part of the signal related to low order modes. The decrease of the energy (increase of attenuation) of the low frequency signal occurs rapidly at sunrise. For the medium

frequency signals (1500–3500 Hz), the attenuation is most visible in latter arrivals, thus associated with higher order modes. In this case the decrease of energy at sunrise is slower than for low frequency signals, but is faster than changes in dissolved O₂ concentration measured by optodes. The variability of the acoustic signal during daytime is high and several peaks and valleys are observed in this period, which suggests the ability of acoustics to detect transient free gas flow occurring during photosynthesis. The signals in the highest band considered in this experiment (6500–8500 Hz) showed a perturbation pattern similar to medium frequency signals in one day, but a different perturbation pattern the next day. Signals in this higher frequency band may be sensitive to other factors that superimpose on water column O₂ effects as for example the sea surface agitation due to wind, as seen during this second day. This issue deserves further investigation. Although the assessment of seagrass primary production by dissolved oxygen measured by optodes and by the changes of acoustic signals are different in nature, a linear relation was apparent between them. However, in this experiment it was not possible to verify the relation during several days, because the geometry of the experiment changed from day to day due to daily recovery and redeployment of hydrophones for maintenance. Nevertheless, hydrophones at various depths (below the middle of the water column) showed similar trends, suggesting that acoustic signature of photosynthesis is independent of the position of the receiver in the water column. The rapid response of acoustic signal that is delayed in the dissolved O₂ measurement by the optodes suggests that O₂ production, and gross primary production by seagrasses might be underestimated by methods that rely on dissolved O₂ changes (input–output mass balance, diel cycle mass balance or eddy covariance). In summary, it was shown that a system based on acoustic methods has the potential to assess the oxygen production of a *P. oceanica* seagrass meadow at the ecosystem level with high temporal resolution. As applicability of the method to meadows of other seagrass species depends on their acoustic behavior, but in principle the method can be adapted for various species.

Acknowledgments

We thank the ESF COST Action (ES 0906) Seagrass Productivity: From Genes to Ecosystem Management for the funds provided and all the participants in the October 2011 WG1 and WG2 Workshop: “linking seagrass productivity, community metabolism, and ecosystem carbon fluxes” for their fruitful contribution; and the STARESO team for logistic support. The transport of the acoustic equipment was supported by project FCT LARSyS (RDO) PEst-OE/EEI/LA0009/2013. O₂ optode mooring was funded by the Fonds National de la Recherche Scientifique (FNRS) (Mandat d'Impulsion Scientifique F.4513.06, Fonds de la Recherche Fondamentale Collective 2.4.511.09 and 2.4.637.10). A.V.B. is a senior research associate at the FNRS. [ST]

References

- Bay, D., 1984. A field study of the growth dynamics and productivity of *Posidonia oceanica* (L.) Delile in Calvi Bay, Corsica. *Aquat. Bot.* 20, 43–64.
- Bonnell, J., Dosso, S., Chapman, R., 2013. Bayesian geoacoustic inversion of single hydrophone light bulb data using warping dispersion analysis. *J. Acoust. Soc. Am.* 134 (1), 120–130.
- Borum, J., Sand-Jensen, K., Binzer, T., Pedersen, O., Greve, T., 2006. Oxygen movement in seagrasses. *Seagrasses: Biology, Ecology and Conservation*. Springer, Netherlands, pp. 255–270.
- Champenois, W., Borges, A.V., 2012. Seasonal and inter-annual variations of community metabolism rates of a *Posidonia oceanica* seagrass meadow. *Limnol. Oceanogr.* 57 (1), 347–361.
- Chipman, L., Huettel, M., Berg, P., Meyer, V., Klimant, I., Glud, R., Wenzhoefer, F., 2012. Oxygen optodes as fast sensors for eddy correlation measurements in aquatic systems. *Limnol. Oceanogr. Methods* 10, 304–316.
- Costanza, R., d'Argue, R., de Groot, R., Farber, S., Grasso, M., Hannon, B., Limburg, K., Naeem, S., O'Neill, R., Paruelo, J., Raskin, R., Sutton, P., van den Belt, M., 1997. The value of the world's ecosystem services and natural capital. *Nature* 387, 253–260.
- Duarte, C., Marba, N., Gacia, E., Fourqurean, J., Beggins, J., Barrón, C., Apostolaki, E., 2010. Seagrass community metabolism: assessing the carbon sink capacity of seagrass meadows. *Glob. Biogeochem. Cycles* 24, 1–8.

- Gazeau, F., Duarte, C.M., Gattuso, J.-P., Barrón, C., Navarro, N., Ruiz, S., Prairie, Y.T., Calleja, M., Delille, B., Frankignoulle, M., Borges, A.V., 2005. Whole-system metabolism and CO₂ fluxes in a Mediterranean bay dominated by seagrass beds (Palma Bay, NW Mediterranean). *Biogeosciences* 2 (1), 43–60.
- Gobert, S., Kyramarios, M., Lepoint, G., Pergent-Martini, C., Bouquegneau, J.-M., 2003. Variations à différentes échelles spatiales de l'herbier *Posidonia oceanica* (L.) Delile; effets sur les paramètres physico-chimiques du sédiment. *Oceanol. Acta* 26 (2), 199–207.
- Gobert, S., Lejeune, P., Chéry, A., Boissery, P., Sartoretto, S., Andral, B., Lepoint, G., Richir, J., 2012. Assessment of the ecological status of *Posidonia oceanica* meadow with a non destructive shoot method. Proceedings of the Mediterranean Seagrass Workshop 2012, Essaouira, Morocco (URL <http://hdl.handle.net/2268/124326>).
- Hecq, J.-H., Bouquegneau, J.-M., Djenidi, S., Frankignoulle, M., Goffart, A., Licot, M., 1986. Some aspects of the liguro-provençal frontal ecohydrodynamics. In: Nihoul, J. (Ed.), *Marine Interfaces Ecohydrodynamics*. Elsevier Oceanography Series vol. 42. Elsevier, pp. 257–271.
- Hermand, J.-P., 2004. Photosynthesis of seagrasses observed in situ from acoustic measurements. *Proc. Int. Conf. IEEE/EOS Oceans'04*, pp. 433–437.
- Hermand, J.-P., Nascetti, P., Cinelli, F., 2000. Inverse acoustical determination of photosynthetic oxygen productivity of *Posidonia* seagrass. In: Caiti, A., Hermand, J.-P., Jesus, S., Porter, M. (Eds.), *Experimental Acoustic Inversion Methods for Exploration of the Shallow Water Environment*. Springer, Netherlands, pp. 125–144.
- Jadot, C., Donnay, A., Acolas, M., Cornet, Y., Anras, M.B., 2006. Activity patterns, home-range size, and habitat utilization of *Sarpa salpa* (Teleostei: Sparidae) in the Mediterranean Sea. *ICES J. Mar. Sci.: J. Cons.* 63 (1), 128–139.
- Lyons, A.P., Abraham, D.A., 1999. Statistical characterization of high-frequency shallow-water seafloor backscatter. *J. Acoust. Soc. Am.* 106 (3), 1307–1315.
- Mackenzie, K.V., 1981. Nine-term equation for sound speed in the oceans. *J. Acoust. Soc. Am.* 70 (3), 807–812.
- Mazzuca, S., Bjork, M., Beer, S., Felisberto, P., Gobert, S., Procaccini, G., Runcie, J., Silva, J., Borges, A.V., Brunet, C., Buapet, P., Champenois, W., Costa, M.M., D'Esposito, D., Gullström, M., Lejeune, P., Lepoint, G., Olivé, I., Rasmunsson, L., Richir, J., Ruocco, M., Serra, I.A., Spadafora, A., Santos, R., 2013. Establishing research strategies, methodologies and technologies to link genomics and proteomics to seagrass productivity, community metabolism and ecosystem carbon fluxes. *Front. Plant Sci.* 4 (38).
- McCarthy, E., Sabol, B., 2000. Acoustic characterization of submerged aquatic vegetation: military and environmental monitoring applications. *OCEANS 2000 MTS/IEEE Conference and Exhibition*. vol. 3, pp. 1957–1961.
- McLeod, E., Chmura, G.L., Bouillon, S., Salm, R., Bjork, M., Duarte, C.M., Lovelock, C.E., Schlesinger, W.H., Silliman, B.R., 2011. A blueprint for blue carbon: toward an improved understanding of the role of vegetated coastal habitats in sequestering CO₂. *Front. Ecol. Environ.* 9 (10), 552–560.
- Medwin, H., Clay, C., 1998. *Fundamentals of Acoustical Oceanography*. Academic Press, USA.
- Munk, W., Worcester, P., Wunsch, C., 1995. *Ocean Acoustic Tomography*. Cambridge University Press.
- Odum, H.T., 1956. Primary production in flowing waters. *Limnol. Oceanogr.* 1, 102–117.
- Pinnegar, J.K., Polunin, N.V., Videler, J.J., de Wiljes, J.J., 2007. Daily carbon, nitrogen and phosphorus budgets for the Mediterranean planktivorous Damselfish *Chromis chromis*. *J. Exp. Mar. Biol. Ecol.* 352 (2), 378–391.
- Roberts, D., Caperon, J., 1986. Lacunar gas discharge as a measure of photosynthesis in seagrasses. *Mar. Ecol. Prog. Ser.* 29, 23–27.
- Roberts, D., Moriarty, D., 1987. Lacunar gas discharge as a measure of productivity in the seagrasses *Zostera capricorni*, *Cymodocea serrulata* and *Syringodium isoetifolium*. *Aquat. Bot.* 28 (2), 143–160.
- MarchSaleiro, M., 2009. Portable acoustic source unit (PASU). Tech. Rep. 05/09. SiPLAB/University of Algarve.
- Silva, J., Sharon, Y., Santos, R., Beer, S., 2009. Measuring seagrass photosynthesis: methods and applications. *Aquat. Biol.* 7.
- Soares, C., Martins, C., Zabel, F., Silva, A., 2011. On the applications of a compact autonomous acoustic recorder. *OCEANS, 2011 IEEE — Spain*, pp. 1–5.
- Staeher, P., Testa, J., Kemp, W.M., Cole, J.J., Sand-Jensen, K., Smith, S., 2011. The metabolism of aquatic ecosystems: history, applications, and future challenges. *Aquat. Sci.* 74, 15–29.
- Tengberg, A., Hovdenes, J., Andersson, H.J., Brocandel, O., Diaz, R., Hebert, D., Arnerich, T., Huber, C., Körtzinger, A., Khripounoff, A., Rey, F., Ronning, C., Schimanski, J., Sommer, S., Stangelmayer, A., 2006. Evaluation of a lifetime-based optode to measure oxygen in aquatic system. *Limnol. Oceanogr.* 4, 7–17.
- Warren, J.D., Peterson, B.J., 2007. Use of a 600-kHz acoustic Doppler current profiler to measure estuarine bottom type, relative abundance of submerged aquatic vegetation, and Eelgrass canopy height. *Estuar. Coast. Shelf Sci.* 72 (1–2), 53–62.
- Waycott, M., Duarte, C.M., Carruthers, T.J.B., Orth, R.J., Dennison, W.C., Olyarnik, S., Calladine, A., Fourqurean, J.W., Heck Jr., K.L., Hughes, A.R., Kendrick, G.A., Kenworthy, W., Short, F.T., Williams, S.L., 2009. Accelerating loss of seagrasses across the globe threatens coastal ecosystems. *Proc. Natl. Acad. Sci. U. S. A.* 106 (30), 12377–12381.
- Wilson, P.S., Dunton, K.H., 2009. Laboratory investigation of the acoustic response of seagrass tissue in the frequency band 0.5–2.5 kHz. *J. Acoust. Soc. Am.* 125 (4), 1951–1959.
- Wilson, C.J., Wilson, P.S., Greene, C.A., Dunton, K.H., 2010. Seagrass leaves in 3-D: using computed tomography and low-frequency acoustics to investigate the material properties of seagrass tissue. *J. Exp. Mar. Biol. Ecol.* 395 (1–2), 128–134.
- Wilson, C.J., Wilson, P.S., Dunton, K.H., 2012. An acoustic investigation of seagrass photosynthesis. *Mar. Biol.* 159 (10), 2311–2322.